PNAS RESEARCH ARTICLE | EVOLUTION

# Detecting environmentally dependent developmental plasticity in fossilized individuals

Anieke Brombacher[a,b,c,1], Alex Searle-Barnes[a], James M. Mulqueeney[a,d], Christopher D. Standish[a], J. Andy Milton[a], Orestis L. Katsamenis[e,f], Richard A. Watson[g], Clive Trueman[a], Ian Sinclair[e,h], Paul A. Wilson[a], Gavin L. Foster[a], and Thomas H. G. Ezard[a]

Affiliations are included on p. 7.

Edited by Nils Stenseth, Universitetet i Oslo, Oslo, Norway; received October 20, 2024; accepted June 10, 2025

**The fossil record provides the most powerful evidence of large-scale biodiversity change on Earth, but it does so at coarse and often idiosyncratic temporal scales. One critical problem that arises concerns the evolutionary consequences of individual environmental experience. Individuals respond to their environment instantaneously, whereas the resolution of most fossil records aggregates multiple paleoenvironments over time scales beyond individual lifespans. Therefore, the presence of phenotypic plasticity in deep time and the extent of its influence on macroevolution remain poorly understood. Using coupled computed tomography and laser ablation inductively coupled plasma mass spectrometry protocols, we studied the environmental dependence of developmental trajectories across three sister species of macroperforate planktonic foraminifera. A foraminiferal shell preserves all stages of the individual's ontogeny, as well as the environmental state experienced throughout its lifetime. Generalized additive mixed effect (GAMM) models show that somatic growth rates differ among the three *Menardella* species and that these are inversely correlated with calcification temperature, as reconstructed from Mg/Ca measurements through ontogeny. This environmental dependence varies among species: The thermal sensitivity of individual chamber-to-chamber growth rates of *Menardella limbata* and *Menardella pertenuis* is double that seen in *Menardella exilis*. In contrast, no such environmental signal was recovered for architectural shape traits. Our integrated approach is widely applicable and demonstrates that detecting developmental plasticity in the fossil record is feasible. Extrapolating these techniques in deep time promises to revolutionize our understanding of the ways in which environmentally associated trait variation drove the diversification of life on Earth.**

developmental plasticity | reaction norm | deep time | planktonic foraminifera

## Significance

Traits are determined by internal factors such as genetics and plastic responses to the external environment. Being able to distinguish which factor most affected the evolution of each trait frames the capacity for organisms to adapt to a changing environment. Most fossils do not carry detailed information on environmental change during their lifetime, but here we study plankton that preserve both their developmental morphological state and their environmental habitat in their shells. We identify environmentally associated trait changes within fossilized individuals from millions of years ago. Our approach can be readily applied to other organisms and help us understand the relative roles of genetically and environmentally associated variation in the origin of new species.

Phenotypic variation forms the basis for micro- and macroevolutionary analysis of the fossil record. Phenotypes form through a combination of genetic and nongenetic components; many genotypes are capable of producing different phenotypes depending on environmental conditions and cues (1). While the fossil record represents an excellent resource for documenting the generation and proliferation of new biodiversity on the largest scales, the common lack of temporal and spatial resolution and the paucity of sufficiently detailed information on the experienced environment have prevented attempts to discriminate how much of the variation in form is environmentally associated (2, 3). Many lines of evidence have been used to speculate that environmentally induced phenotypic plasticity, the capacity of a single genotype to give rise to multiple phenotypes, introduces new variation and therefore has the potential to promote speciation (4, 5). There is growing evidence that phenotypic variation shapes species divergence in deep time (6), but the lack of empirical data means that the role of phenotypic plasticity in macroevolutionary change remains unknown (7–9).

Ecophenotypic, i.e. environmentally associated, variation is often invoked to explain morphological variation in the fossil record (3), but widely accepted evidence is currently lacking. Phenotypic plasticity in modern analogue species is sometimes used to argue for similarly plastic traits in fossil ancestors (e.g., refs. 10, 11–13), but most fossil species do not have modern analogues and, in those that do, the same phenotypic differences can be both environmentally and genetically controlled (14, 15). A high degree of morphological variation within a species (16–21), or morphological variation among populations in different environmental settings (13, 16, 22–26) has often been ascribed to ecophenotypic variation in the fossil record but a purely genetic basis for this variation cannot be ruled out from studying morphology alone (27–29). To quantify the potential adaptability of form in fossil species and determine how much of that versatility flows from environmental influence (3), it is necessary to calculate how much of that variability is environmentally associated.

Author contributions: T.H.G.E. designed research; A.B., A.S.-B., and J.M.M. performed research; C.D.S., J.A.M., O.L.K., R.A.W., C.T., I.S., P.A.W., and G.L.F. contributed new reagents/analytic tools; A.B. analyzed data; and A.B. wrote the paper.

The authors declare no competing interest.

This article is a PNAS Direct Submission.



[1]To whom correspondence may be addressed. Email: Anieke.Brombacher@noc.ac.uk.

This article contains supporting information online at https://www.pnas.org/lookup/suppl/doi:10.1073/pnas.2421549122/-/DCSupplemental.

Published July 3, 2025.

In extant populations, hypotheses concerning the balance between plastic and genetic trait changes are tested either through experimental manipulation of genetically identical individuals or by gathering repeated measurements on the same individuals experiencing different environments through their lifetimes (30, 31). In the fossil record, the most obvious limiting factor in establishing the extent to which variability results from plastic or genetic properties is the lack of coupled contemporaneous environmental data at sufficient fine-scale temporal resolution. Changes in ontogenetic trajectories (16, 21, 26, 32, 33) or the degree of asymmetry in ontogenetic trajectories (24, 34) have been argued to indicate environmentally associated variation in deep time, but these approaches cannot rule out purely genetic variation. To partition trait variation into genetic and environmentally associated components, we need detectable morphological and environmental signals at biologically relevant temporal resolutions.

Here, we map life history and shell architecture traits of individuals in three species of planktonic foraminifera (*Menardella limbata, Menardella exilis,* and *Menardella pertenuis*, *SI Appendix*, Fig. 1) to the environments experienced by individuals during their life. Each foraminifer grows by adding a new calcite chamber to its overall shell as a discrete ontogenetic stage every few days (Fig. 1). We develop repeatable, high-resolution laboratory-based protocols to map morphological developmental trajectories extracted from X-ray microcomputed tomography (CT, Fig. 1) (35) to the changing environment through the life of each fossil individual as recorded in the calcite Mg/Ca ratios and measured through laser ablation inductively coupled plasma mass spectrometry (LA-ICP-MS) (36, 37). We compare individual ontogenetic trajectories from developmental stage $t$ to stage $t + 1$ to ambient temperature recorded in the calcite Mg/Ca ratios at stage $t$. We then aggregate these repeated morphology-environment associations into generalized additive mixed models to build environmental reaction norms in deep time and determine how much trait variation is best explained by an individual's response to the environmental changes it experienced millions of years ago.

## 1. Results

*Menardella pertenuis* reaches a larger final size than its ancestor *M. limbata* (two-sample $t$ test, t = 2.48, df = 16.82, $P$ = 0.012, Fig. 2*A*) with two more chambers on average (two-sample $t$ test, t = 3.37, df = 22.47, $P$ = 0.0014). *Menardella exilis* is smaller (two-sided $t$ test, t = 4.03, df = 28.10, $P < 0.001$) and has one less chamber on average (two-sided $t$ test, t = 2.13, df = 43.98, $P$ = 0.019) than *M. limbata*. All three species are characterized by high growth rates early in ontogeny, which decrease later in life (Fig. 2*B*). Growth rates of descendants *M. exilis* and *M. pertenuis* remain lower than those of *M. limbata* early in ontogeny and decrease at a later stage and at larger shell volume than their ancestor. Angles between subsequent chambers do not change detectably through ontogeny for *M. exilis* but increase later in life for *M. limbata* and *M. pertenuis* (Fig. 2*C*). Trochospirality does not differ detectably throughout ontogeny for all studied species (Fig. 2*D*).

Variation in chamber-to-chamber growth rates through an individual's life is best explained by the generalized additive mixed model (GAMM) as a species-specific ontogenetic response to the Mg/Ca temperature proxy (model 7, Table 1); models that instead include internal constraints such as ontogeny (models 2 and 3) and cumulative volume (models 4 and 5) have markedly lower support. The linear mixed effect components of the GAMM showed no detectable impact of species-specific somatic growth rates versus the nested null model, unlike Model 6, which incorporated a general environmental response to ln(Mg/Ca) across all species, and Model 7, which incorporated both the general linear relationship between ln(Mg/Ca) and the nonlinear species-specific environmental response (Table 1). This species-specific environmental response model also outperformed the general environmental response model. Within an individual's life, each unit increase in ln(MgCa), which corresponds to a temperature change of ~6.4 ± 0.9%/°C (38), is associated with an average change in chamber-to-chamber growth rate of −0.0795 (SE = 0.0283, t = −2.81, $P < 0.01$). The species-specific environmental model explained ~9% more variation than the general environmental response model (adjusted $r^2$ of 0.537 and 0.491, respectively). The higher Akaike weights of models that link ambient temperature at stage $t$ to growth from stage $t$ to $t + 1$ in our fossil individuals (Table 1) is evidence that these species differ not only in their overall morphology (Fig. 2) but how the environment shapes each individual's growth trajectory (Fig. 3).

With respect to the architectural traits, chamber-to-chamber angles within individuals are affected by the volume of the existing

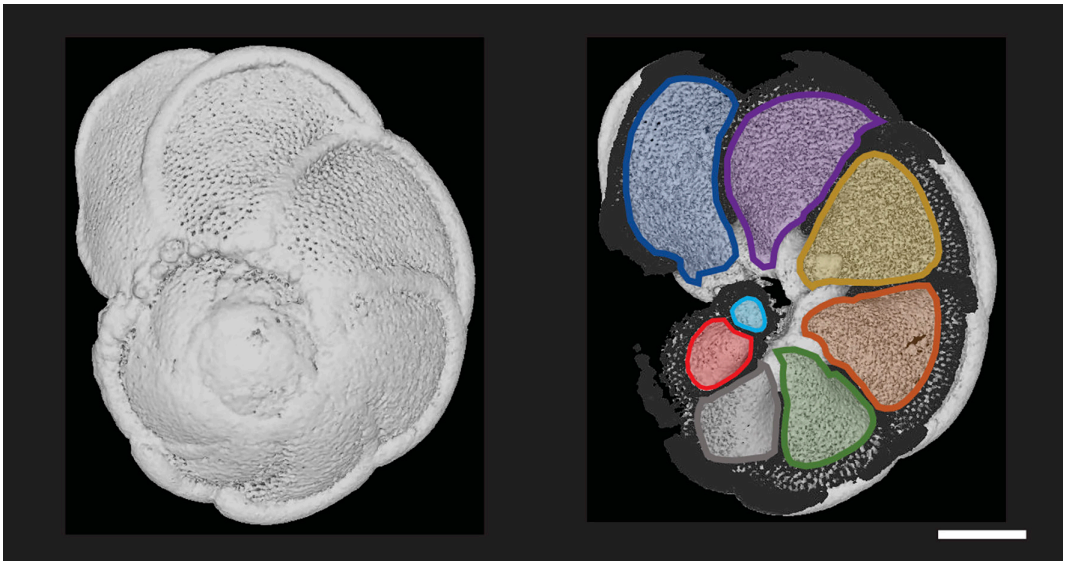

**Fig. 1.** CT scan of *Menardella limbata* specimen (*Left*) and a 3D reconstruction of a cross-section of the same specimen with individual chambers highlighted in different colors (*Right*). The scale bar represents 100 μm. Visualized in Dragonfly version 2021.3 (Object Research Systems, Canada).

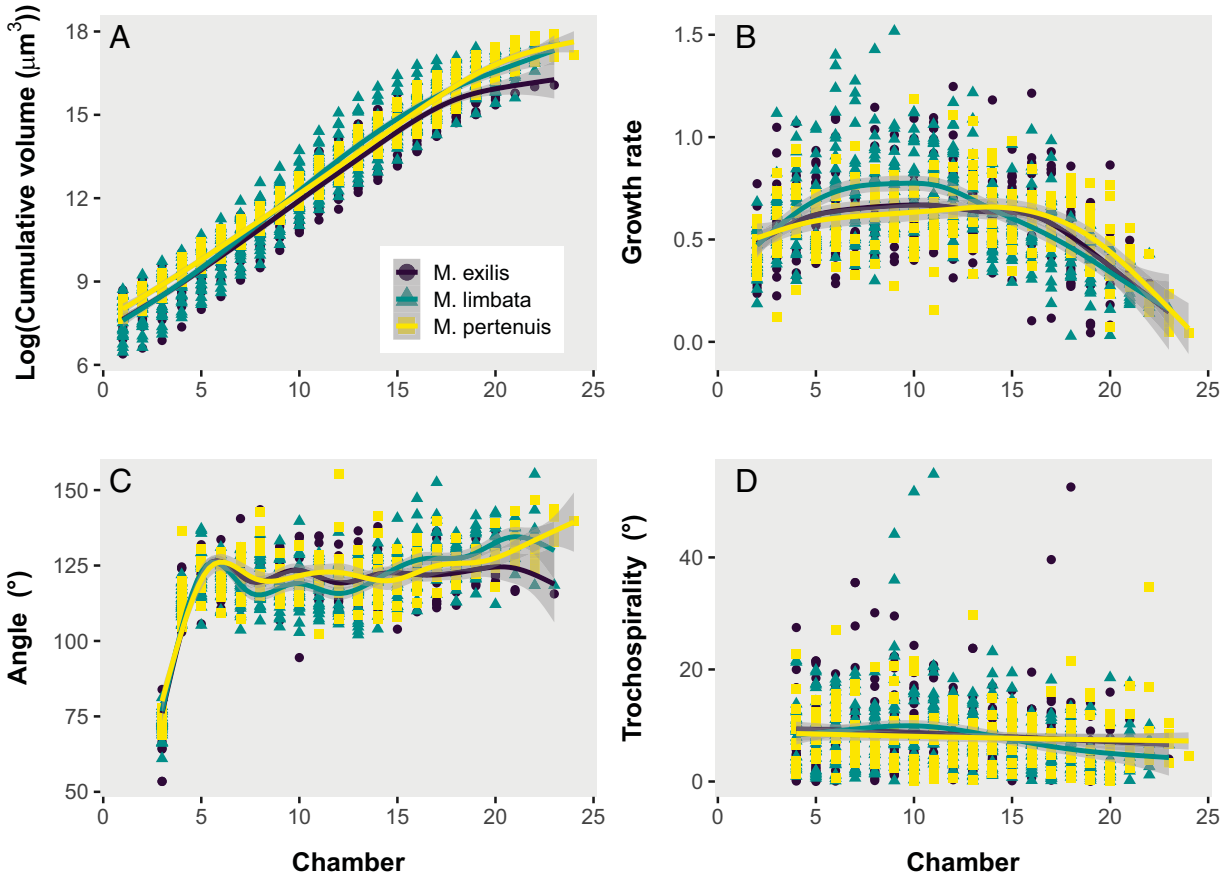


**Fig. 2.** Cumulative volume (*A*), growth rates (*B*), chamber angles (*C*), and trochospirality (*D*) throughout ontogeny for *Menardella limbata*, *Menardella exilis,* and *Menardella pertenuis*. Smooth lines represent generalized additive model results, with shaded areas for the models' 95% CI.

shell at the time the chamber was built (i.e., stage *t*), not detectably by ambient temperature at stage *t*, and the nonlinearity of the relationships varies among species (Table 2). Trochospirality is also affected by the volume of the existing shell at the time the chamber was built, not detectably by ambient temperature at stage *t* and without any clear species-specific relationships (Table 3).

In all species, somatic growth rate slows toward the terminal (reproductive) life stage but the rate of slowing depends on species-specific responses to temperature as documented by ln(Mg/Ca) of the focal chamber. Growth rates among species are most similar at lowest temperatures (lowest Mg/Ca values). Model-averaged predictions show that chamber-to-chamber growth rates in *M. exilis* are less affected by temperature changes through life than either *M. limbata* or *M. pertenuis. Menardella limbata* and *M. pertenuis* exhibit lower somatic growth when temperatures are higher (Fig. 3). The LA-ICP-MS measurements are highly repeatable: The uncertainty associated with repeated measurements of the same chamber is five orders of magnitude smaller than that associated with repeated measurements across chambers of the same individual ($3.88*10^{-6}$ and 0.06, respectively), which implies that within-chamber Mg/Ca variation is negligible compared to among-chamber, i.e. through ontogeny, Mg/Ca variation.

While differential environmental dependence of *M. limbata* and *M. pertenuis* is not detectable through ln(Mg/Ca) reaction norm differentiation, *M. pertenuis* grows a calcite shell that is less than 90% of the thickness of either *M. exilis* or *M. limbata* (gamma generalized linear model with inverse link function, $\beta = 0.00396$, SE = 0.00137, $P < 0.05$; Fig. 4). Together these variations indicate environmentally dependent developmental plasticity throughout the life of these organisms as individuals within the three species respond to their environments in detectably different ways.

## 2. Discussion

We show a reconstruction of species-specific environmental dependencies throughout the life cycle of fossil individuals. Despite differences in chamber-to-chamber growth rates among species, ontogenetic stage was not the best predictor for growth rate variation (Table 1). Instead, the Mg/Ca temperature proxy for each ontogenetic stage *t* markedly improved predictions of chamber-to-chamber growth from stage *t* to stage *t* + *1* (Fig. 3). While the overall dependence of growth on temperature agrees with patterns seen in biogeographic size distributions (39, 40) and in physiological models (41), we detect weaker environmental sensitivity in *M. exilis* than either *M. limbata* or *M. pertenuis* (Fig. 3).

In contrast to growth rates, the parameters describing the shape of the shell growth spiral show very little response to external influences (Tables 2 and 3). Angles between subsequent chambers depend mainly on the total volume of the shell at the time the chamber was built, with specific relationships varying among species. For *M. limbata* and *M. pertenuis*, angles remain stable through the first half of ontogeny, followed by a gradual increase in the second half of their life. One explanation of this result is linked to a change in growth rate, with relatively smaller chambers completing a smaller section of the whorl and so increasing angles between chambers, but the model including growth rates as a response variable does not explain the data as well as the model with cumulative volume (Table 2). This suggests that, regardless

**Table 1. Generalized additive mixed effect (GAMM) model results of Menardella chamber growth rate response to internal and external processes**

| Model | Degrees of freedom | $r^2$ | AIC | ΔAIC | Akaike weight |
|---|---|---|---|---|---|
| **m7: species-specific responses to Mg/Ca** | **9** | **0.538** | **−403.3** | **0** | **0.959** |
| m6: similar response to Mg/Ca across all species | 8 | 0.491 | −396.1 | 7.17 | 0.027 |
| m8: similar response to temperature with ontogenetic differences across all species | 9 | 0.492 | −394.6 | 8.67 | 0.013 |
| m2: similar response to chamber size across all species | 7 | 0.484 | −389.1 | 14.16 | 0.001 |
| m3: species-specific responses to chamber size | 8 | 0.485 | −388.2 | 15.1 | 0.001 |
| m4: similar response to cumulative volume across all species | 7 | 0.371 | −291.3 | 111.93 | 0 |
| m5: species-specific responses to cumulative volume | 8 | 0.377 | −290.2 | 113.1 | 0 |
| m1: fixed differences across species, without change through ontogeny | 5 | 0 | −111.5 | 291.76 | 0 |
| m0: random effects only | 5 | 0 | −111.5 | 291.76 | 0 |

Log likelihoods that feed into AIC scores are presented based on maximum likelihood calculations from the linear mixed effect part of the GAMM to facilitate comparisons among fixed effects; random effects for all models were specimen and laser blast (where the same chamber was repeatedly measured to assess instrument consistency). Adjusted r2 calculations are drawn from the generalized additive model part of the GAM. ΔAIC represents the difference between AIC and the set's minimum AIC. The best performing model based on lowest AIC and highest Akaike weight is indicated in bold. All models include autocorrelation within specimens, and specimens and laser shots as random effects. The best performing model includes a general linear relationship with ln(Mg/Ca), as a linearized proxy for temperature of the calcification environment, and a species-specific nonlinear spline between Mg/Ca and species classification.

of temperature-associated growth variation, individuals adjust chamber their shape to maintain their overall spiral shape.

Planktonic foraminifera are known to show temperature-dependent chamber-to-chamber growth rates (42, 43). They reproduce at the end of their life by transforming all cell cytoplasm into gametes (36) and individuals must grow large enough to produce enough gametes quickly enough to reduce the chance of death before reproduction. Growth is limited by the energetic cost of calcification (41). This trade-off between costs and benefits of high growth rates results in different life-history trajectories among species: While *M. limbata* and *M. exilis* have indistinguishable environmental sensitivities, the descendant *M. pertenuis* reaches the same overall size using <90% calcite in its shell. The canonical view of *Menardella* depth habitat through ontogeny includes reproduction in the pycnocline (~30 to 40 m water depth depending on region), followed by downward migration to up to 400 m water depth, and ending with mature specimens ascending back to the pycnocline for reproduction (44). Water temperature decreases with depth, so this would suggest a strong relationship between ontogenetic stage and Mg/Ca, but we do not see this in our data (Table 1, model 7). Meilland, Siccha, Kaffenberger, Bijma, and Kucera (45) also reported that more than half of the planktonic foraminifera they encountered in plankton tows did not follow classic depth habitat patterns, suggesting large variation in depth habitat within ontogenetic stages. If temperature is indeed the largest determinant of chamber-to-chamber growth rate, then variation in depth habitat increases variation in calcification temperature. Given chamber-to-chamber growth is the major determinant of population growth (46), the temperature dependence we report here is closely linked to mean population fitness for this life history.

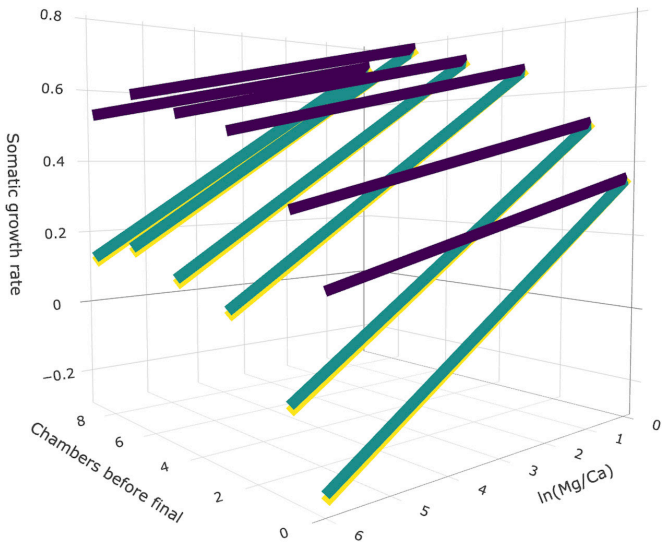


**Fig. 3.** Generalized additive mixed model results for somatic growth rates, plotted against both chamber number (ontogenetic stage) and Mg/Ca. Note that "chambers before final" indicates ontogenetic growth stage counting back because individuals grow various numbers of chambers (e.g., Fig. 2) and the experimental control is to count back from the final (terminal) growth stage.

Our framework for detecting deep time environmentally associated changes in morphological traits throughout the life cycle of fossilized individuals shows that studying developmental plasticity in the fossil record is feasible. Our observations open a door to help determine whether environmentally associated phenotypic plasticity is involved in driving macroevolutionary change (3). Saulsbury et al. (47) showed how the internal variational properties predict individual growth rates more strongly than external abiotic factors across 195 species of living marine bivalves, while Palmer, Moss, Surge, and Turek (48) showed that mid- to high-latitude bivalves were more impacted by abiotic changes than low latitude individuals. Neither of these studies were able to break down the growth rate analysis into discrete ontogenetic stages because they lacked the contemporaneous environmental resolution we show here. Our approach supersedes these previous approaches because it allows us to detect the existence of environmentally associated developmental plasticity (Fig. 3). Given model predictions that increasing developmental plasticity would increase mean population fitness (46), future investigations might investigate whether species tolerances to temperature are due to changing environmental associations within individuals through ontogeny, or rather across individuals through populations, and whether that environmental association changes before, during, or after speciation.

Levis and Pfennig (7) proposed four criteria to investigate plasticity-led evolution: the opportunity to (1) detect environmentally dependent plastic traits in ancestral and derived

**Table 2. GAMM model results of Menardella chamber angle in response to internal and external processes**

| Model | Degrees of freedom | $r^2$ | AIC | ΔAIC | Akaike weight |
|---|---|---|---|---|---|
| **m5: species-specific responses to cumulative volume** | **8** | **0.27** | **3,126** | **0** | **0.916** |
| m4: similar response to cumulative volume across all species | 7 | 0.236 | 3,130.8 | 4.78 | 0.084 |
| m7: species-specific response to Mg/Ca | 9 | 0.174 | 3,158.1 | 32.11 | 0 |
| m3: species-specific responses to chamber size | 8 | 0.098 | 3,158.7 | 32.66 | 0 |
| m2: similar response to chamber size across all species | 7 | 0.122 | 3,159.6 | 33.58 | 0 |
| m8: similar response to temperature with ontogenetic differences across all species | 9 | 0.096 | 3,160.7 | 34.66 | 0 |
| m6: similar response to Mg/Ca across all species | 8 | 0.12 | 3,161.6 | 35.57 | 0 |
| m9: similar response to growth rate across all species | 7 | 0.147 | 3,177.4 | 51.36 | 0 |
| m10: species-specific response to growth rate | 8 | 0.147 | 3,179.4 | 53.36 | 0 |
| m1: fixed differences across species, without change through ontogeny | 7 | 0.059 | 3,202.5 | 76.47 | 0 |
| m0: random effects only | 5 | 0 | 3,212.2 | 86.22 | 0 |

Log likelihoods that feed into AIC scores are presented based on maximum likelihood calculations from the linear mixed effect part of the GAMM to facilitate comparisons among fixed effects; random effects for all models were specimen and laser blast (where the same chamber was repeatedly measured to assess instrument consistency). Adjusted r2 calculations are drawn from the generalized additive model part of the GAM. ΔAIC represents the difference between AIC and the set's minimum AIC. The best performing model based on lowest AIC and highest Akaike weight is indicated in bold. All models include autocorrelation within specimens, and specimens and laser shots as random effects. The best performing model includes a general and species-specific nonlinear spline as a function of cumulative shell volume to the time of calcification.

lineages and (2) reconstruct reaction norms through time with (3) a sufficient sample size to detect an increase in trait variation following environmental changes and (4) sufficient resolution to track mean changes in the focal trait. Our approach, using high-resolution fossil records that preserve ontogenetic stages and environmental variation at the time of growth, fulfills these criteria and can be readily extended to other calcifying marine organisms that preserve both environmental and ontogenetic information in their skeletons. Ammonoids are a prime example, preserving both ontogeny and environmental information (e.g., ref. 49). Additionally, corals and bivalves have long been used to reconstruct past sea surface temperature, salinity, and pH (e.g., refs. 50, 51). Combining their growth layers with the environmental information stored within them can reveal valuable information on their potential for adaptation in changing environments. Finally, fossil bryozoans, colonial marine organisms that have existed since the Ordovician, contain information on both their life history and environment (52), and are known to exhibit developmental plasticity in response to changing environmental conditions (53).

If trait-based approaches are to provide a more mechanistic route to understanding species vulnerabilities (54, 55), then generalizing the contributions of environmentally associated trait variation is an achievable goal to span both the differences in temporal scope among data (56) and the timeframes of fossil preservation and necessary conservation action (54). The ability to extract the lived environment of organisms in time-averaged fossil samples is not only reassuring for the adequacy of temporal age models but also provides a quantitative metric of the sources of the morphological variation (27–29). The Levis and Pfennig (7) criteria were not set out explicitly for paleontological systems, but the acceleration of geochemical and imaging technologies, alongside the integration of methodological advancements used in this study, now provide exciting opportunities to investigate how environmentally associated trait variation contributed to the generation, proliferation, and extinction of life on Earth.

**Table 3. GAMM model results of Menardella trochospirality in response to internal and external processes**

| Model | Degrees of freedom | $r^2$ | AIC | ΔAIC | Akaike weight |
|---|---|---|---|---|---|
| **m4: similar response to cumulative volume across all species** | **7** | **0.036** | **2,947.6** | **0** | **0.615** |
| m5: species-specific responses to cumulative volume | 8 | 0.043 | 2,949.3 | 1.71 | 0.262 |
| m9: similar response to growth rate across all species | 7 | 0.023 | 2,952.6 | 5.07 | 0.049 |
| m0: random effects only | 5 | 0 | 2,954.5 | 6.97 | 0.019 |
| m10: species-specific response to growth rate | 8 | 0.023 | 2,954.6 | 7.07 | 0.018 |
| m2: similar response to chamber size across all species | 7 | 0.006 | 2,955.9 | 8.35 | 0.009 |
| m6: similar response to Mg/Ca across all species | 8 | 0.006 | 2,955.9 | 8.33 | 0.01 |
| m1: fixed differences across species, without change through ontogeny | 7 | 0.01 | 2,956.2 | 8.64 | 0.008 |
| m3: species-specific responses to chamber size | 8 | 0.006 | 2,957.9 | 10.35 | 0.003 |
| m7: species-specific response to Mg/Ca | 9 | 0.006 | 2,957.9 | 10.33 | 0.004 |
| m8: similar response to temperature with ontogenetic differences across all species | 9 | 0.006 | 2,957.9 | 10.33 | 0.004 |

Log likelihoods that feed into AIC scores are presented based on maximum likelihood calculations from the linear mixed effect part of the GAMM to facilitate comparisons among fixed effects; random effects for all models were specimen and laser blast (where the same chamber was repeatedly measured to assess instrument consistency). Adjusted r2 calculations are drawn from the generalized additive model part of the GAM. ΔAIC represents the difference between AIC and the set's minimum AIC. The best performing model based on lowest AIC and highest Akaike weight is indicated in bold. All models include autocorrelation within specimens, and specimens and laser shots as random effects. The best performing model includes a general nonlinear spline as a function of cumulative shell volume to the time of calcification.

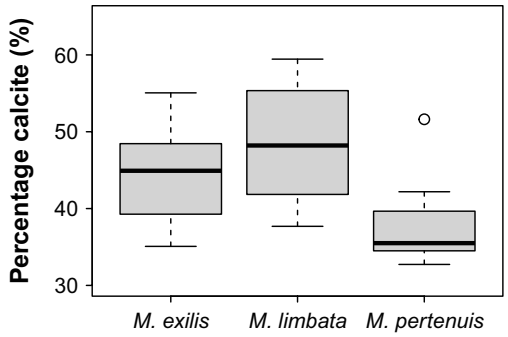


**Fig. 4.** Percentage calcite of the total shell volume for *Menardella limbata*, *Menardella exilis,* and *Menardella pertenuis*.

## 3. Methods

**3.1. Study Species.** We studied the Neogene planktonic foraminifera species *Menardella limbata* and its two descendent species *Menardella exilis* and *Menardella pertenuis* (*SI Appendix*, Fig. 1), which originated in the Pliocene, ~4.5 and ~3.5 Mya (57). All three species are exclusively found in tropical and warm subtropical waters. Their shells are characterized by lenticular, low trochospiral tests with a prominent keel (58). *Menardella exilis* and *M. pertenuis* can be distinguished from *M. limbata* by a thinner, "shinier" shell and lower trochospire, with *M. pertenuis* additionally possessing a thin plate extending over the umbilicus and more chambers in the final whorl than *M. exilis* (58). All three species became extinct between 2.6 and 2.2 Ma (57), shortly after Earth had cooled sufficiently to promote the waxing and waning of large ice sheets on North America and Eurasia for the first time in the Cenozoic era (59, 60).

**3.2. Study Site.** Ocean Drilling Program (ODP) Site 925 is located in the western equatorial Atlantic at a water depth of 3,040 m (4° 12′ N, 43° 29′ W), well above the local carbonate lysocline (61). The age model for Site 925 was recently updated by high-resolution benthic oxygen isotope stratigraphy (62). The site sits in the core of the biogeographic range of all three study species, which are found in high abundance in Pliocene sediments (57). The first appearance dates of *M. exilis* and *M. pertenuis* are well documented at Site 925 (57) and agree with global low-latitude biostratigraphic schemes (63, 64).

We analyzed five time slices: one before the origination of *M. exilis* and *M. pertenuis*, one during the speciation of *M. exilis*, one after the origination of *M. exilis* but before the origination of *M. pertenuis*, one during the speciation of *M. pertenuis*, and one when all three species had become established. For every time slice, we analyzed 3 to 8 specimens of all species occurring in that time slice. Sediment samples were dry-sieved over a >150 μm mesh sieve and divided using a microsplitter. Specimens were selected for CT scanning through assignment of random numbers to avoid further biases.

**3.3. Micro-CT Scanning and 3D Shell Model Reconstruction.** To maximize throughput, prior to CT scanning specimens were stacked one on top of the other separated by ~2 mm layers of polyurethane foam in transparent plastic drinking straws (2 mm diameter). The foam and plastic straw have significantly lower attenuation properties compared to foraminiferal calcite which makes it easy to exclude from the CT data. This allowed individual identification for subsequent geochemical work and programming of a multiscan session. Scans were conducted at the μ-VIS X-ray Imaging Centre, University of Southampton, UK by a Versa 510 X-ray microscope (Carl Zeiss Microscopy GmbH, Germany) using a tungsten transmission target, a peak voltage of 110 kV at 10 W and a 0.15 mm SiO2 glass filter to reduce beam hardening artifacts. Two-stage magnification was achieved by utilizing a 4× objective. To increase the signal-to-noise ratio, the detector was binned twice, resulting in a voxel resolution of 1.75 μm. Each scan was focused on a single specimen and imaged using 1,011 projections at 1.3 s exposure time per radiograph projection. The projection data were then reconstructed using a sharp reconstruction filter with a beam hardening correction of 1.0 to further reduce beam hardening artifacts into a 16-bit tiff stack [32 to 16-bit window: (−0.04, 0.10)] characterized by an average dimension of 992 × 1,015 pixels for each 2D slice using the Zeiss XM FBP Reconstruction software (Carl Zeiss Microscopy GmbH, Germany).

**3.4. Three-Dimensional Growth Analyses.** We analyzed three-dimensional growth trajectories of all scanned foraminifera focusing on ecologically relevant life-history traits (46, 65). We use chamber number as an indicator of ontogenetic stage and calculate size at each ontogenetic stage *t* as the sum of the volumes of all chambers present at the time chamber *t* was built. To reconstruct individual chambers, all specimen CT scans were processed using Dragonfly [66 (version 2021.3)]. Each specimen's volume data were imported into Dragonfly where the XY, XZ, and YX planes were manually aligned to the specimen's proloculus centroid. Using both the smart grid tool and manual brush we labeled each chamber's internal area on a slice-by-slice basis (Fig. 1). All ROIs assigned to a single chamber were combined into a multi-ROI layer, for which Dragonfly calculated the volume and the *x*, *y,* and *z* centroid coordinates. Ten specimens were analyzed by two members of the team to assess repeatability; the mean proportion of variation explained by a regression across the two repeats of chamber volume was 0.977 (range across specimens from 0.912 to 0.999). All final data presented come from a single operator who repeated all measurements for the fullest consistency.

Chamber-to-chamber (somatic) growth rates were calculated as the increase in total shell volume for every chamber added relative to the size at the previous chamber addition. To analyze spiral growth in three dimensions, we extracted centroid coordinates of all chambers from the Dragonfly specimen reconstructions. Using the foram3D package (65) in R, version 4.2.1 (R Core 67) we calculated the angle a chamber makes with the previous two chambers, and trochospirality at each ontogenetic step, where trochospirality is the angle a chamber is added at relative to the plane spanned by the previous three chambers [see figure 11 in Brombacher, Searle-Barnes, Zhang, and Ezard (65)]. Changes in the angle of new chamber addition point to changes in the number of chambers in the final whorl, a key diagnostic feature for *Menardella* species, whereas trochospirality is known to change with ontogenetic stages such as the transition from juvenile to neanic and could thus be used to quantify growth stages (68–74).

**3.5. Laser Ablation Inductively Coupled Plasma Mass Spectrometry.** We use Mg/Ca ratios in the foraminiferal chamber calcite as a proxy for temperature at the time of chamber formation as foraminiferal calcite Mg/Ca ratios increase with ambient temperature (75, 76). Although specific temperature-Mg/Ca relationships vary among species (75) and these curves are impossible to parameterize experimentally for extinct species, for the purpose of this study, the positive correlation between temperature and Mg/Ca is sufficient to investigate the effect of temperature on ontogenetic trajectories within individuals of our sister species.

Mg/Ca ratios were determined using laser ablation inductively coupled plasma mass spectrometry (LA-ICP-MS). Following CT scanning, specimens were mounted on glass slides using double-sided adhesive tape. Trace elements in the foraminiferal calcite were analyzed using an Agilent (Agilent Technologies Inc., CA, USA) 8900 triple quadrupole inductively coupled plasma (QQQ-ICP) mass spectrometer coupled to an Elemental Scientific Lasers (Bozeman, MT, USA) NWR193 excimer laser ablation system at the School of Ocean and Earth Science, University of Southampton. The following isotopes were acquired in time resolved mode: $^{7}$Li, $^{9}$Be, $^{11}$B, $^{24}$Mg, $^{27}$Al, $^{43}$Ca, $^{44}$Ca, $^{55}$Mn, $^{65}$Cu, $^{66}$Zn, $^{88}$Sr, $^{137}$Ba, and $^{238}$U (only $^{24}$Mg and $^{44}$Ca are presented here). The final chamber (f), penultimate chamber (f-1), and chamber f-3 were ablated in two separate locations to quantify within-chamber variation (see also Kearns et al. 2023). Chambers f-5, f-7, and f-9 were ablated in a single location due to limited area.

Each ablation was performed using a 30 μm diameter spot, with a repetition rate of 5 Hz at a fluence of 0.73 J/cm$^{2}$. Each acquisition was preceded by a 15-s gas blank/laser warmup and was followed by a 30-s "wash" (to permit residual material to leave the system). Ten replicates of NIST 612 and 610 reference glasses, a pressed powder pellet of MACS-3 (United States Geological Survey), and a pressed powder pellet of JCp-1 (Porites sp. coral, Japanese Geological Survey) were analyzed in batches throughout each analysis session after every 80 to 100 analyses.

Each time-resolved analysis was background subtracted using the gas blank measured immediately before each sample (or standard). Sample and standard data were internally normalized using Ca wt% using the following concentrations: 37.7 wt% MACS-3, 37.5 wt% JCp-1, 8.5 wt% NIST 612, and 8.15 wt% NIST 610 (77, 78). Elemental concentrations in the chamber walls were determined using a calibration derived from NIST 612, NIST 610, and MACS-3 (reference concentrations from ref. 77). Following ref. 79, a pressed powder pellet of JCp-1 was

analyzed as an unknown to assess accuracy (using the same calibration strategy). Average concentrations in JCp-1 were determined as follows: Mg was 836 ± 124 ppm (vs. 867 ± 23 ppm in ref. 77) and Ca was 38.1 ± 3.8% Ca [vs. 37.5 ± 2.4% by Sekimoto et al. (80)]. After calibration, our NIST glass calibrations thus predict trace elements within carbonate target material within the specified uncertainty limits. Trace element ratios were extracted using the lablaster R package (81) and presented as the median of all on-target time slices, applying the endPoint function (dt = 10, smoothing = 10) to identify when the laser fully penetrated the chamber wall.

**3.6. Statistical Analyses.** To investigate the effects of internal and external constraints on *Menardella* growth rates and morphology within and among species, we employed generalized additive mixed models (GAMMs) using the "mgcv" package (82) in R [version 4.2.1 R Core Team (67)]. GAMMs consist of two parts: a linear mixed effect part and a generalized additive model part. Growth rates, trochospirality, and chamber angles were modeled as potentially nonlinear spline relationships against: i) chamber number (ontogenetic stage), ii) cumulative volume (to investigate for size thresholds for changes in growth rates), and iii) Mg/Ca ratios as indicator of temperature of the calcification environment during the lived life-cycle of the now fossil individual. The models for trochospirality and chamber angles additionally included growth rates as fixed effect to investigate possible dependency of architectural traits on growth rates. Specimen ID code and laser shots (in the case of multiple shots of the same chamber) were included as random effects in all models to facilitate model comparisons using Akaike Information Criterion values (AIC) (83). The species-level splines were specified using an "interactive" fixed effect between the explanatory variables above and the species classification. Splines were penalized using the default settings. If models with the species-specific spline performed better than those without, then there is evidence that the effect of environment (via the Mg/Ca proxy) on ontogenetic trajectories differs among species. The best performing model of those fitted has the lowest AIC, which combines deviance explained and the number of parameters used, and thus the highest Akaike weight (83). All R code used to fit the models and output results tables are available as a *SI Appendix*.

**Data, Materials, and Software Availability.** Ontogenetic and environmental data in a .xlsx file R code for the statistical analyses in a .R file data have been deposited in Figshare (https://doi.org/10.6084/m9.figshare.27260970) (84).

**ACKNOWLEDGMENTS.** We thank two anonymous reviewers for their constructive feedback on an earlier version of this manuscript. This study was funded by the Natural Environment Research Council (NE/P019269/1). We acknowledge μ-VIS X-ray Imaging Centre (https://muvis.org), part of the National Facility for laboratory-based X-ray CT (nxct.ac.uk–EPSRC: EP/T02593X/1) at the University of Southampton for the provision of the μCT imaging, processing, and data management infrastructure.

Author affiliations: [a]School of Ocean and Earth Science, University of Southampton, Southampton SO14 3ZH, United Kingdom; [b]Department of Earth and Planetary Sciences, Yale University, New Haven, CT 06511; [c]Division of Science and Technology, National Oceanography Centre, Southampton SO14 3ZH, United Kingdom; [d]Department of Life Sciences, Natural History Museum, London SW7 5BD, United Kingdom; [e]μ-VIS X-ray Imaging Centre, Faculty of Engineering and the Environment, University of Southampton, Southampton SO17 1BJ, United Kingdom; [f]Institute for Life Sciences, University of Southampton, Southampton SO17 1BJ, United Kingdom; [g]Electronics and Computer Science, University of Southampton Highfield Campus, Southampton SO17 1BJ, United Kingdom; and [h]Engineering Materials, Faculty of Engineering and Physical Sciences, University of Southampton, Southampton SO17 1BJ, United Kingdom

1. R. C. Lewontin, *The Genetic Basis of Evolutionary Change* (Columbia University Press, New York, USA, 1974).
2. G. J. Vermeij, Biological versatility and Earth history. *Proc. Natl. Acad. Sci. U.S.A.* **70**, 1936–1938 (1973).
3. A. C. Love *et al.*, Evolvability in the fossil record. *Paleobiology* **48**, 1–24 (2022).
4. M. J. West-Eberhard, Developmental plasticity and the origin of species differences. *Proc. Natl. Acad. Sci. U.S.A.* **102**, 6543–6549 (2005).
5. M. J. West-Eberhard, *Developmental Plasticity and Evolution* (Oxford University Press, New York, 2003).
6. A. Holstad *et al.*, Evolvability predicts macroevolution under fluctuating selection. *Science* **384**, 688–693 (2024).
7. N. A. Levis, D. W. Pfennig, Evaluating "Plasticity-First" evolution in nature: Key criteria and empirical approaches. *Trends Ecol. Evol.* **31**, 563–574 (2016).
8. N. A. Levis, D. W. Pfennig, Plasticity-led evolution: A survey of developmental mechanisms and empirical tests. *Evol. Dev.* **22**, 71–87 (2020).
9. D. J. Futuyma, Evolutionary biology today and the call for an extended synthesis. *Interface Focus* **7**, 1–13 (2017).
10. S. J. Hageman, M. M. Bayer, C. D. Todd, Partitioning phenotypic variation: Genotypic, environmental and residual components from bryozoan skeletal morphology. *J. Nat. Hist.* **33**, 1713–1735 (1999).
11. D. H. Geary, An unusual pattern of divergence between two fossil gastropods: Ecophenotypy, dimorphism, or hybridization? *Paleobiology* **18**, 93–109 (1992).
12. E. M. Standen, T. Y. Du, H. C. Larsson, Developmental plasticity and the origin of tetrapods. *Nature* **513**, 54–58 (2014).
13. S. C. Antón, C. W. Kuzawa, Early homo, plasticity and the extended evolutionary synthesis. *Interface Focus* **7**, 1–15 (2017).
14. D. M. Raup "Approaches to morphologic analysis" in *Models in Paleobiology*, T. J. M. Schopf, Ed. (Freeman & Cooper, San Francisco, USA, 1972), pp. 28–44.
15. K. F. Darling, M. Kucera, D. Kroon, C. M. Wade, A resolution for the coiling direction paradox in *Neogloboquadrina pachyderma*. *Paleoceanography* **21**, 1–14 (2006).
16. P. M. Sander, N. Klein, Developmental plastcity in the life history of a prosauropod dinosaur. *Science* **310**, 1800–1802 (2005).
17. T. M. Cronin, C. E. Schneider, Climatic influences on species: Evidence from the fossil record. *Trends Ecol. Evol.* **5**, 275–279 (1990).
18. G. Fryer, P. H. Greenwood, J. F. Peake, Punctuated equilibria, morphological stasis and the palaeontological documentation of speciation: A biological appraisal of a case history in an African lake. *Biol. J. Linn. Soc.* **20**, 195–205 (1983).
19. G. Fryer, P. H. Greenwood, J. F. Peake, The demonstration of speciation in fossil molluscs and living fishes. *Biol. J. Linn. Soc.* **26**, 325–336 (1985).
20. A. Kin, Early Maastrichtian ammonites and nautiloids from Hrebenne, southeast Poland, and phenotypic plasticity of *Acanthoscaphites tridens* (Kner, 1848). *Cretaceous Res.* **31**, 27–60 (2010).
21. B. M. Gee, Y. Haridy, R. R. Reisz, Histological skeletochronology indicates developmental plasticity in the early Permian stem lissamphibian *Doleserpeton annectens*. *Ecol. Evol.* **10**, 2153–2169 (2020).
22. G. P. Lohmann, B. A. Malmgren, Equatorward migration of *Globorotalia truncatulinoides* ecophenotypes through the Late Pleistocene: Gradual evolution or ocean change? *Paleobiology* **9**, 414–421 (1983).
23. J. F. Dynowski, J. H. Nebelsick, Ecophenotypic variations of *Encrinus liliiformis* (Echinodermata: Crinoidea) from the middle Triassic Muschelkalk of Southwest Germany. *Swiss J. Palaeontol.* **130**, 53–67 (2010).
24. N. Schlüter, Ecophenotypic variation and developmental instability in the Late Cretaceous echinoid *Micraster brevis* (Irregularia; Spatangoida). *PLoS One* **11**, 1–26 (2016).
25. R. R. Schoch, Life cycles, plasticity and palaeoecology in temnospondyl amphibians. *Palaeontology* **57**, 517–529 (2014).
26. S. Sanchez, A. de Ricqlès, R. Schoch, J. S. Steyer, Developmental plasticity of limb bone microstructural organization in Apateon: Histological evidence of paedomorphic conditions in branchiosaurs. *Evol. Dev.* **12**, 315–328 (2010).
27. A. M. Lister, "Phenotypic plasticity in the fossil record" in *Phenotypic Plasticity and Evolution*, D. W. Pfennig, Ed. (CRC Press, Boca Raton, 2021), chap. 11, pp. 267–297.
28. D. Jablonski, Developmental bias, macroevolution, and the fossil record. *Evol. Dev.* **22**, 103–125 (2020).
29. I. S. C. Jackson, Developmental bias in the fossil record. *Evol. Dev.* **22**, 88–102 (2020).
30. V. Oostra, M. Saastamoinen, B. J. Zwaan, C. W. Wheat, Strong phenotypic plasticity limits potential for evolutionary responses to climate change. *Nat. Commun.* **9**, 1–11 (2018).
31. A. Charmantier *et al.*, Adaptive phenotypic plasticity in response to climate change in a wild bird population. *Science* **320**, 800–803 (2008).
32. A. L. A. Johnson, Detection of ecophenotypic variation in fossils and its application to a Jurassic scallop. *Lethaia* **14**, 277–285 (1981).
33. N. C. Hughes, Morphological plasticity and genetic flexibility in a Cambrian trilobite. *Geology* **19**, 913–916 (1991).
34. M. Webster, Morphological homeostasis in the fossil record. *Semin. Cell Dev. Biol.* **88**, 91–104 (2019).
35. D. N. Schmidt, E. J. Rayfield, A. Cocking, F. Marone, Linking evolution and development: Synchrotron radiation X-ray tomographic microscopy of planktic foraminifers. *Palaeontology* **56**, 741–749 (2013).
36. C. Hemleben, M. Spindler, O. R. Anderson, *Modern Planktic Formaminifera* (Springer, New York, 1989).
37. S. Eggins, P. De Deckker, J. Marshall, Mg/Ca variation in planktonic foraminifera tests: Implications for reconstructing palaeo-seawater temperature and habitat migration. *Earth Planet. Sci. Lett.* **212**, 291–306 (2003).
38. W. R. Gray, D. Evans, Nonthermal influences on Mg/Ca in planktonic foraminifera: A review of culture studies and application to the last glacial maximum. *Paleoceanogr. Paleoclimatol.* **34**, 306–315 (2019).
39. A. D. Hecht, An ecologic model for test size variation in recent planktonic foraminifera: Applications to the fossil record. *J. Foraminiferal Res.* **6**, 295–311 (1976).
40. S. Renaud, D. N. Schmidt, Habitat tracking as a response of the planktic foraminifer Globorotalia truncatulinoides to environmental fluctuations during the last 140 kyr. *Mar. Micropaleontol.* **49**, 97–122 (2003).
41. M. Grigoratou *et al.*, A trait-based modelling approach to planktonic foraminifera ecology. *Biogeosciences* **16**, 1469–1492 (2019).
42. F. Lombard *et al.*, Modelling planktic foraminifer growth and distribution using an ecophysiological multi-species approach. *Biogeosciences* **8**, 853–873 (2011).
43. F. Lombard, L. Labeyrie, E. Michel, H. J. Spero, D. W. Lea, Modelling the temperature dependent growth rates of planktic foraminifera. *Mar. Micropaleontol.* **70**, 1–7 (2009).
44. R. Schiebel, C. Hemleben, Modern planktic foraminifera. *Paläontol. Z.* **79**, 135–148 (2005).
45. J. Meilland, M. Siccha, M. Kaffenberger, J. Bijma, M. Kucera, Population dynamics and reproduction strategies of planktonic foraminifera in the open ocean. *Biogeosciences* **18**, 5789–5809 (2021).
46. A. Brombacher, D. N. Schmidt, T. H. G. Ezard, Developmental plasticity in deep time: A window to population ecological inference. *Paleobiology* **49**, 259–270 (2023).

47. J. Saulsbury *et al.*, Evaluating the influences of temperature, primary production, and evolutionary history on bivalve growth rates. *Paleobiology* **45**, 405–420 (2019).
48. K. L. Palmer, D. K. Moss, D. Surge, S. Turek, Life history patterns of modern and fossil *Mercenaria* spp. from warm vs. cold climates. *Palaeogeogr. Palaeoclimatol. Palaeoecol.* **566**, 110227 (2021).
49. J. A. Sessa *et al.*, Ammonite habitat revealed via isotopic composition and comparisons with co-occurring benthic and planktonic organisms. *Proc. Natl. Acad. Sci. U.S.A.* **112**, 15562–15567 (2015).
50. D. M. Thompson, Environmental records from coral skeletons: A decade of novel insights and innovation. *WIREs Clim. Change* **13**, 1–40 (2021).
51. N. J. De Winter *et al.*, Absolute seasonal temperature estimates from clumped isotopes in bivalve shells suggest warm and variable greenhouse climate. *Commun. Earth Environ.* **2**, 1–8 (2021).
52. A. M. Smith, "Palaeonenvironmental interpretations using bryozoans: A review" in *Marine Palaeoenvironmental Analysis from Fossils*, D. W. J. Bosence, P. A. Allison, Eds. (The Geological Society, Geological Society London, 1995), **vol. 83**, pp. 231–243.
53. C. Lombardi, S. Cocito, M. C. Gambi, P. D. Taylor, Morphological plasticity in a calcifying modular organism: Evidence from an *in situ* transplant experiment in a natural CO2 vent system. *R. Soc. Open Sci.* **2**, 1–12 (2015).
54. W. Kiessling, J. A. Smith, N. B. Raja, Improving the relevance of paleontology to climate change policy. *Proc. Natl. Acad. Sci. U.S.A.* **120**, 1–7 (2023).
55. A. D. Barnosky *et al.*, Merging paleobiology with conservation biology to guide the future of terrestrial ecosystems. *Science* **355**, 1–10 (2017).
56. M. E. Clapham, Conservation evidence from climate-related stressors in the deep-time marine fossil record. *Philos. Trans. R. Soc. Lond. B Biol. Sci.* **374**, 1–7 (2019).
57. W. Chaisson, P. N. Pearson, "Planktonic foraminifer biostratigraphy at site 925: Middle miocene-pleistocene" in *Proceedings of the Ocean Drilling Program, Scientific Results*, N. J. Shackleton, Ed. (1997), vol. 154, pp. 3–31.
58. J. P. Kennett, M. S. Srinivasan, *Neogene Planktonic Foraminifera. A phylogenetic atlas* (Hutchinson Ross Publishing Company, Stroudsburg, Pennsylvania, 1983).
59. I. Bailey *et al.*, An alternative suggestion for the Pliocene onset of major Northern Hemisphere glaciation based on the geochemical provenance of North Atlantic Ocean ice-rafted debris. *Quat. Sci. Rev.* **75**, 181–194 (2013).
60. J. F. Spray *et al.*, North Atlantic evidence for a unipolar icehouse climate state at the Eocene-Oligocene transition. *Paleoceanogr. Paleoclimatol.* **34**, 1124–1138 (2019).
61. W. B. Curry, N. J. Shackleton, C. Richter, "Expedition 154 Scientists, Site 925" in *Proceedings of the Ocean Drilling Program, Initial Reports* (1995), vol. 154.
62. R. H. Wilkens *et al.*, Revisiting the Ceara Rise, equatorial Atlantic Ocean: Isotope stratigraphy of ODP leg 154 from 0 to 5 Ma. *Clim. Past* **13**, 779–793 (2017).
63. B. S. Wade, P. N. Pearson, W. A. Berggren, H. Pälike, Review and revision of Cenozoic tropical planktonic foraminiferal biostratigraphy and calibration to the geomagnetic polarity and astronomical time scale. *Earth-Sci. Rev.* **104**, 111–142 (2011).
64. D. J. King, B. S. Wade, R. D. Liska, C. G. Miller, A review of the importance of the Caribbean region in Oligo-Miocene low latitude planktonic foraminiferal biostratigraphy and the implications for modern biogeochronological schemes. *Earth-Sci. Rev.* **202**, 1–27 (2020).
65. A. Brombacher, A. Searle-Barnes, W. Zhang, T. H. G. Ezard, Analysing planktonic foraminiferal growth in three dimensions with foram3D: An R package for automated trait measurements from CT scans. *J. Micropalaeontol.* **41**, 149–164 (2022).
66. Object Research Systems (ORS) Inc, *Dragonfly* (Montreal, Canada, 2022).
67. R. C. Team, *R: A language and environment for statistical computing* (R Foundation for Statistical Computing, Vienna, Austria, 2023).
68. G.-J.A. Brummer, C. Hemleben, M. Spindler, Planktonic foraminiferal ontogeny and new perspectives for micropalaeontology. *Nature* **319**, 50–52 (1986).
69. G.-J.A. Brummer, C. Hemleben, M. Spindler, Ontogeny of extant spinose planktonic foraminifera (Globigerinidae): A concept exemplified by *Globigerinoides sacculifer* (Brady) and *G. ruber* (d'Orbigny). *Mar. Micropaleontol.* **12**, 357–381 (1987).
70. A. G. Caromel, D. N. Schmidt, I. Fletcher, E. J. Rayfield, Morphological change during the ontogeny of the planktic foraminifera. *J. Micropalaeontol.* **35**, 2–19 (2016).
71. M. Apthorpe, Middle Jurassic (Bajocian) planktonic foraminifera from the northwest Australian margin. *J. Micropalaeontol.* **39**, 93–115 (2020).
72. S. Kendall, F. Gradstein, C. Jones, O. T. Lord, D. N. Schmidt, Ontogenetic disparity in early planktic foraminifers. *J. Micropalaeontol.* **39**, 27–39 (2020).
73. C. R. Poole, B. S. Wade, Systematic taxonomy of the *Trilobatus sacculifer* plexus and descendant *Globigerinoidesella fistulosa* (planktonic foraminifera). *J. Syst. Palaeontol.* **17**, 1989–2030 (2019).
74. R. Morard *et al.*, Genetic and morphological divergence in the warm-water planktonic foraminifera genus Globigerinoides. *PLoS One* **14**, 1–30 (2019).
75. D. W. Lea, T. A. Mashiotta, H. J. Spero, Controls on magnesium and strontium uptake in planktonic foraminifera determined by live culturing. *Geochim. Cosmochim. Acta* **63**, 2369–2379 (1999).
76. D. Nürnberg, J. Bijma, C. Hemleben, Assessing the reliability of magnesium in foraminiferal calcite as a proxy for water mass temperature. *Geochim. Cosmochim. Acta* **60**, 803–814 (1996).
77. K. P. Jochum *et al.*, High-resolution Mg/Ca measurements of foraminifer shells using femtosecond LA-ICP-MS for paleoclimate proxy development. *Geochem. Geophys. Geosyst.* **20**, 2053–2063 (2019).
78. K. P. Jochum *et al.*, Determination of reference values for NIST SRM 610–617 glasses following ISO guidelines. *Geostand. Geoanal. Res.* **35**, 397–429 (2011).
79. L. E. Kearns *et al.*, The influence of geochemical variation among *Globigerinoides ruber* individuals on paleoceanographic reconstructions. *Paleoceanogr. Paleoclimatol.* **38**, 1–20 (2023).
80. S. Sekimoto *et al.*, Neutron activation analysis of carbonate reference materials: Coral (JCp-1) and giant clam (JCt-1). *J. Radioanal. Nucl. Chem.* **322**, 1579–1583 (2019).
81. A. Searle-Barnes, J. A. Milton, C. D. Standish, G. L. Foster, T. H. G. Ezard, Laser ablation mass spectrometry blast through detection in R. *Rapid Commun. Mass Spectrom.* **37**, 1–8 (2023).
82. S. N. Wood, Fast stable restricted maximum likelihood and marginal likelihood estimation of semiparametric generalized linear models. *J. R. Stat. Soc. Ser. B Stat. Methodol.* **73**, 3–36 (2011).
83. A. F. Zuur, E. N. Ieno, N. Walker, A. A. Saveliev, G. M. Smith, "Mixed effect models and extensions in ecology with R" in *Statistics for Biology and Health*, M. Gail, K. Krickeberg, J. M. Samet, A. Tsiatis, W. Wong, Eds. (Springer-Verlag, New York, NY, 2009).
84. A. Brombacher *et al.*, Data from 'Detecting environmentally dependent developmental plasticity in fossilised individuals'. Figshare. https://doi.org/10.6084/m9.figshare.27260970. Deposited 19 May 2025.